

# The influence of admixture on chloride time-varying diffusivity and microstructure of concrete by low-field NMR



Junzhi Zhang, Jie Guo, Denghui Li, Yurong Zhang\*, Fan Bian, Zhaofeng Fang

College of Civil Engineering and Architecture, Zhejiang University of Technology, No. 18 Chaowang Road, Xiacheng District, Hangzhou 310014, PR China

## ARTICLE INFO

**Keywords:**  
Concrete  
Chloride  
Admixture  
Diffusion coefficient  
Micro-structure  
NMR

## ABSTRACT

The permeability of chloride can be used as an important indicator of durability. In this article, based on the ingress test in an artificial simulating dry-wet cycling chloride environment, the influence of four minerals, namely basalt fiber (BF), fly ash (FA), silica fume (SF), and combined FA and SF mixture on the penetration of chloride ions and microstructure in concrete were examined. In addition, the chloride diffusion coefficients of concrete were fitted with Fick's diffusion law, and pore characteristic parameters and pore-size distribution with exposure time were measured by a nuclear magnetic resonance (NMR) technology. The results show that the addition of these mineral admixtures can increase anti-permeability and decrease properties of concrete at the same exposure time. Moreover, the addition of SF has the most obvious decreasing effect on porosity, and the decreased effect of FA on chloride diffusion coefficient of concrete is the most significant, especially at the later stage. Minerals can refine the pore-size distribution in concrete, in which the content of aperture radius 100~1000 nm pores decreases after the same exposure time. At last, we can also see that the influence of contributive porosity of aperture radius 100~1000 nm in concrete on chloride diffusion coefficient is more than that of total porosity of concrete, there is a better positive correlation between contributive porosities of radius 100~1000 nm in concrete and chloride diffusion coefficients.

## 1. Introduction

Chloride ingress into concrete is an issue of the durability of reinforced concrete (RC) structures (Yu et al., 2015). The corrosion of reinforcing steel is the most common cause of premature deterioration and failure of concrete, leading to a reduction of its service life, particularly for structures exposed to deicing salt or marine environment (Papakonstantinou and Shinozuka, 2013). The study on the reinforcing steel corrosion in concrete is a complex process, depending on many factors, including not only the concrete materials itself (e.g. the admixture, the quality of concrete and the type of reinforcement) but also the environmental factors (e. g. exposure condition, temperature and humidity) (Valipour et al., 2014). Pore micro-structure in concrete plays an important role for its mechanical and durability properties (Pipilikaki and Beazi-Katsion, 2009). The transport properties of cement-based materials are related to many factors such as the porosity, size and connectivity of capillary pores. Decreasing the porosity is the most important issue to improve the durability of RC structures (Gao et al., 2013). Therefore, many researchers have focused their studies on the porosity of concrete materials (Jia et al., 2016). Various methods, such as reducing water

to binder ratio and adding mineral admixtures etc., have been employed to decrease the permeability of concrete by reducing the porosity (Mohammed et al., 2014; Camacho et al., 2014). However, the durability failure of a RC structure is a long and slow process and can be affected by many factors, most of which are time-dependent (Simčič et al., 2015; Song et al., 2013). Costa and Appleton (1999) calibrated the parameters of Fick's second law of diffusion by using a long term chloride ion penetration experiment of concrete in the marine environment, in which an age factor was defined to express the time-dependent characteristic of chloride diffusion coefficients in concrete (Boddy et al., 1999; Mangat and Molloy, 1994; Audenaert et al., 2010). Mangat and Molloy (1994) and Tang and Nilsson (1995) used rapid diffusivity tests and field data to obtain the variation of the diffusion coefficient with time, respectively. Zhang and Ye (2010) studied the influences of age and w/c ratio on the chloride diffusion coefficient. Existing results revealed that the chloride diffusion coefficient has a decrease trend with the increased exposure time or the decreased w/c ratio when the concrete is exposed to the chloride environment (Costa and Appleton, 1999; Boddy et al., 1999; Mangat and Molloy, 1994; Audenaert et al., 2010; Tang and Nilsson, 1995; Zhang and Ye, 2010; Khanzadeh-Moradillo et al., 2015).

\* Corresponding author.

E-mail address: [zhangyr1988@126.com](mailto:zhangyr1988@126.com) (Y. Zhang).

It is well-known that the resistance of concrete to chloride ingress is largely related to the chloride diffusion coefficient and the porosity of concrete. Some methods, such as the mercury intrusion porosimetry (MIP), electric flux and ASTM C1202, were often used to investigate the chloride diffusion coefficient and the micro-structure of concrete. It was reported that MIP measurements are useful to provide threshold diameters and intrudable pore space measurements, which can be served as comparative indices for the connectivity and capacity of the pore systems in hydrated cements (Cook and Hover, 1999; Loukili et al., 1999; Zhang, 1998; Diamond, 2000). However, it is difficult to provide precisely quantitative relation or correlation between micro-structure and diffusion performance of concrete by using these methods. Recently, nuclear magnetic resonance (NMR) technology has been used to determine the quantitative relation between ionic diffusion coefficient and pore micro-structure parameters (Wang et al., 2015). Today, the low field NMR can be used as a useful way for the traditional methods to characterize the pore structure of concrete.

In the present study, a new method based on the low field NMR is developed to study the time-varying relationship between the porosity and pore-size distribution and the chloride diffusion coefficient in concrete. Based on an artificial simulation experiment, the effects of three represented mineral admixtures of basalt fiber (BF), fly ash (FA), silica fume (SF) and a ternary mixture of FA and SF on penetration of chloride ions in concrete were analyzed. NMR was used to investigate the porosity and micro-pore size distribution in tested concrete. In addition, the effects of exposure time and the amount of mineral admixtures on chloride diffusion coefficient and micro-pore size distribution in concrete were analyzed. The results showed that NMR is very effective in examining the micro-pore structure of large size concrete specimen. Moreover, it can be used to study the relationship between time-varying diffusivity and microstructure in concrete.

## 2. Materials and testing methods

### 2.1. Materials and mix proportion of tested concrete

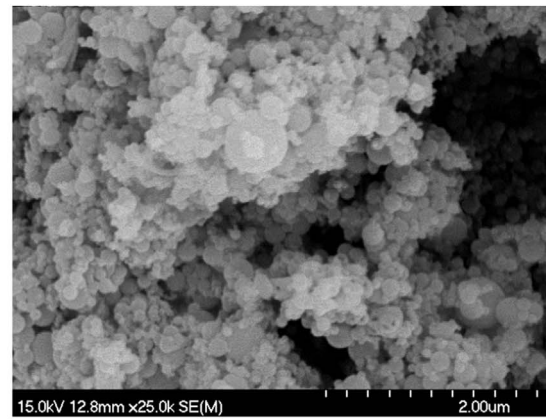
Common river sand is used as fine aggregates in this experiment. The fineness modulus of the sand is 2.4 with an apparent density of 2600 kg/m<sup>3</sup>. The maximum size of coarse aggregates is 31.5 mm with an apparent density of 2700 kg/m<sup>3</sup>. The cement used in the tested concrete is Qian-Chao complex Portland cement (PC 32.5) with a density of 3100 kg/m<sup>3</sup>. The water used in the mix as well as for curing is the laboratory tap water.

The admixtures used in tested concrete include the chopped basalt fiber (BF) with filament diameter 17–20 μm and tensile strength 390–450 MPa, the silica fume (SF) with Bertrand specific area 21,000 m<sup>2</sup>/kg, 350 mesh and 91.3% SiO<sub>2</sub>, and the fly ash (FA) with fineness 4.6% and apparent density of 2240 kg/m<sup>3</sup> and specific surface area 454 m<sup>2</sup>/kg. Fig. 1 shows the SEM images of SF with particle size 0.01–0.03 μm and stair FA with particle size 1–10 μm, and the photo of BF with length 17–24 mm.

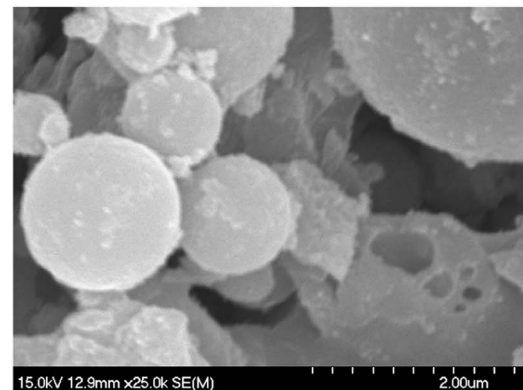
The weight of water used in the tested concrete mixes is 190 kg/m<sup>3</sup>, which gives the constant water-to-binder ratio 0.5. The ratio of fine to coarse aggregates used in the mixes is purposely kept to be 32% for reducing the influence of raw material randomness on the experimental results. The details of the mixture proportions of tested concrete are summarized in Table 1.

### 2.2. Concrete producing

The specimen of the tested concrete was made in accordance with the Chinese standards of SL352-2006. Five cylindrical specimens of size Φ100 × 50 mm were used for chloride ingress test and nuclear magnetic resonance (NMR) test for each concrete mixture. After 24 h of the specimens being cast, they were demoulded placed into a



(a) SEM image of magnified 25,000 times SF



(b) SEM image of magnified 25,000 times stair FA



(c) Photo of BF with length 17~24 mm

Fig. 1. SEM images and photo of materials used in the test.

standard curing room for a period of 28 days with the temperature of 20 °C ± 5 °C and relative humidity of 95%. After the 28 days curing, the cylindrical specimens were used for chloride exposure test to examine the variation of pore structure of the mixed concrete.

**Table 1**  
Concrete mixture proportions.

Code	Content (kg/m <sup>3</sup> )						w/c	
	C	FA	SF	BF	Aggregate <sup>e</sup>			W
					F	C		
A1	380.0	—	—	—	578	1229	190	0.50
A2 <sup>a</sup>	380.0	—	—	1.03	578	1229	190	0.50
A3 <sup>b</sup>	361.0	—	19	—	578	1229	190	0.50
A4 <sup>c</sup>	304.0	76	—	—	578	1229	190	0.50
A5 <sup>d</sup>	304.0	57	19	—	578	1229	190	0.50

<sup>a</sup> A2: 0.3% by volume of cement, which is 1.03 kg/m<sup>3</sup>.  
<sup>b</sup> A3: Cement replacement SF, 5% by weight of 380 kg cement.  
<sup>c</sup> A4: Cement replacement FA, 20% by weight of 380 kg cement.  
<sup>d</sup> A5: Cement replacement FA and SF, 20% and 5% by weight of 380 kg cement, respectively.  
<sup>e</sup> Fine aggregates (F): 100% w/w passing an 8 mm sieve, 96.5% w/w passing a 4 mm sieve. Coarse aggregates (C): 100% w/w passing a 40 mm sieve, 40% w/w passing a 16 mm sieve.

2.3. Exposure environment and testing methods

2.3.1. Exposure environment

The exposure experiment of cylindrical specimens was carried out under an artificial simulated environment, which is to simulate a natural marine tidal zone in Zhou Shan, Zhejiang, China. Before the specimens were put into the artificial simulated environment, the side surface and one circular surface of the specimens were sealed using epoxy resin, which leaves only one circular surface to expose to the seawater environment. Fig. 2 shows a sketch of the exposure experiment.

Four different artificial environmental factors were set to simulate the changes of four seasons in the local marine tidal zone. In order to accelerate the ingress process of chloride ions in the specimens, the artificial simulated temperature was set twice as high as the average one of the corresponding season in Zhou Shan. Table 2 shows the temperature and humidity data used in each season in the simulated test.

According to the data obtained from the local seawater test, the weight ionic concentration of chlorides in the seawater in Zhou Shan was about 1.27%. Using the NaCl solution to simulate the seawater, the average concentration of NaCl solution would be as 2.1%. In order to accelerate the ingress of chloride ions into concrete, a rather high concentration of NaCl solution of 12.5% in weight was used in the test. The specimens were exposed to the artificial environment, which

**Table 2**  
Environmental parameters of artificial climate for marine tidal range.

Parameters/seasons	Spring	Summer	Autumn	Winter
Temperature (°C)	29	52	40	40
Humidity (%)	80	85	85	76

includes 4 h immersion in the NaCl solution, followed by 44 h of drying for every 48 h (two days) exposure for a total of 240, 320 or 400 days exposure tests.

2.3.2. Measurement of free chloride ion concentrations in concrete

After the expected exposure time was reached, the specimens were taken to the laboratory from the site, and grinded into powder starting from the exposed surface into the inside of the specimen with 2 mm interval by using a concrete grinding miller. Then, the powder was kept for 2 h in a 150 °C oven after sieving with 0.63 mm screen and cooled down in indoor temperature to measure the concentration of free chloride ions. The powder sample at each depth having a mass of approximately 6–8 g was selected to measure the content of chloride ions, in which the weighing precision for powder sample with an electronic balance is 0.001 g.

An experimental test is made for chloride content in tested concrete before official testing the content of chloride ions, with the aims to understand the least time of separating out chloride ions and the stability of the test apparatus, so as to determine the test plan and method. According to the study of comparison, the solution after 48 h of mixing is a good one for testing, so the test time for content of free chloride ions in concrete with the acidometer is 48 h later after mixing the standard solution (Zhang et al., 2010).

When conducting the test of the free chloride concentration, the mass of beaker ( $m_1$ ) is weighed first. Then adding a certain amount of powder (generally 2–6 g) to the empty beaker and weighting their mass, denoted as  $m_2$ . Third, preparing solution (100 mL) by adding the sample powder into the deionized water (distilled water) and weighting their mass, denoted as  $m_3$ . Vibrating the solution for 1–2 min and then mixing 2 mL ions stabilizer (ISA) into the solution. At last, the free chloride content in the above 100 mL solution can be measured by using the THERMO Orion DUAL Star PH acidometer, the reading is recorded as  $p$ . The measured free chloride concentration  $\omega$  is the mass percentage of chloride to concrete, as shown in the following.

$$\omega = 0.0001 \times p \times \frac{(m_3 - m_2)}{(m_2 - m_1)} \tag{1}$$

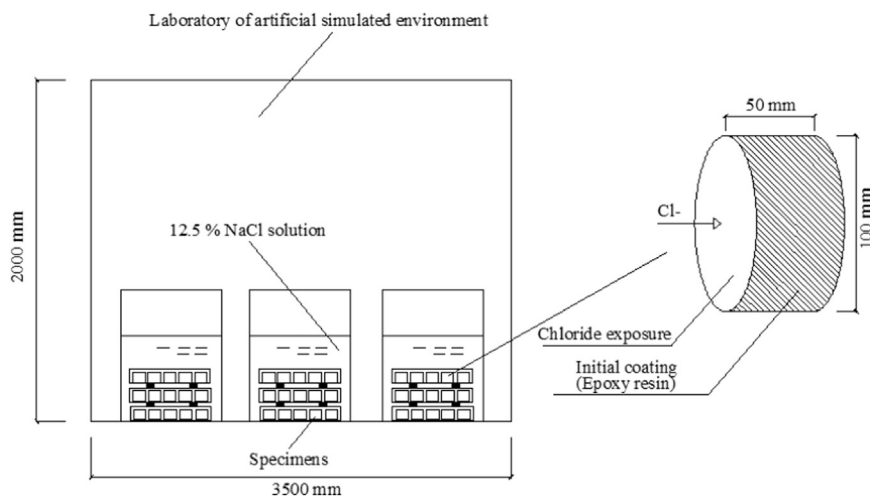


Fig. 2. Experimental process.

### 2.4. Porosity testing

#### 2.4.1. Preparation of specimens

In order to examine the correlation between the diffusion of chloride ions and the microstructure in concrete, after milling powder, all samples used for the NMR test of pore structure were retained, in the cylinders of 100 mm diameter and 20 mm height. First of all, the brush was used to clear the dust on the surface. Second, the specimens were put into distilled water for 16 h at the vacuum pressure of 0.1 MPa in order to make the water saturate the specimens fully, which is the most important step to ensure the accuracy of the test results. Third, the specimens were taken out from the water, wipe off the moisture on the surface and wrap it with preservative films. At last, the specimens were put into the magnet coil to carry out the NMR test.

#### 2.4.2. Testing principle

NMR technique has been commonly used in the field of oil exploration and rock materials to analyze the porosity, pore structure, pore size distribution and pore water content (Jaeger et al., 2009; Xiao, 1998). Although there is a big difference in pore structure between rock materials and concrete, the related researches on pore structure of concrete have been carried out (Wang et al., 2015; Dong et al., 2015).

NMR is used to measure the signal of hydrogen proton in the sample. The hydrogen protons are in the state of spin which make it as a micro magnet (Tian et al., 2014). Within a fixed external magnetic field, all protons will tend to align along with the direction of the magnetic field (Jaeger et al., 2009). An external radio frequency (RF) pulse will impose to the magnetic field. After reaching a stable state, the RF will revoke. The protons will go through a process of turning back to the initial state which is called relaxation. The relaxation is divided into transverse relaxation and longitudinal relaxation. The time required to complete the transverse relaxation process is called transverse relaxation time ( $T_2$ ). According to the relationship between nuclear magnetic signal and  $T_2$ , the porosity and pore size distribution can be obtained (Ji et al., 2015).

In the porous structure, the  $T_2$  of hydrogen protons is related to the bulk relaxation time ( $T_{2B}$ ), surface relaxation time ( $T_{2S}$ ) and diffusion relaxation time ( $T_{2D}$ ) (Tian et al., 2014; Coates et al., 1999), which can be presented as

$$\frac{1}{T_2} = \frac{1}{T_{2S}} + \frac{1}{T_{2B}} + \frac{1}{T_{2D}} \quad (2)$$

In a water-saturated porous structure and short echo time (TE), the  $T_{2S}$  dominates the relaxation time  $T_2$  (Bayer et al., 2010). Eq. (2) can thus be simplified as

$$\frac{1}{T_2} \approx \frac{1}{T_{2S}} = \rho_2 \frac{A}{V} \quad (3)$$

where  $\rho_2$  is the  $T_2$  surface relativity, A is the area of the pore wall and V is the fluid volume.

According to the assumption of the shape of the pore, Eq. (3) can be further simplified as

$$\frac{1}{T_2} = \rho_2 \frac{F}{R} \quad (4)$$

where R is the pore radius and F is a shape factor, which can be assumed to be equal to 1, 2 and 3 for planar, cylindrical and spherical pores, respectively (Tian et al., 2014).

From Eq. (4), we can see that there is a linear relationship between  $T_2$  and pore size. Hence, if  $T_2$  is known, the porosity and the distribution of pores can be analyzed.

#### 2.4.3. Testing instrument

The instrument (Macro-MR12-150H, Niumag Electric Corporation, Suzhou, China) with a constant magnetic field of 0.3 T and a radio-frequency coil of 150 mm in diameter, operating at 12.797 MHz, was used for the low-field NMR experiments in this study. Different parameter

**Table 3**  
Parameters setting of low-field NMR.

Parameters	TE ( $\mu$ m)	TW ( $\mu$ m)	NS	NECH	PRG
Values	0.2	2000	64	18,000	2

settings in the NMR equipment will lead to different results. Therefore, an experiment was taken at the beginning to confirm the minimum error parameters, including repeated sampling waiting time (TW), echo number (NECH), echo time (TE), number of scans (NS) and pre-amp gain (PRG). Table 3 shows the optimized results.

#### 2.4.4. Calibrating

The test results may also be affected by factors such as temperature and magnetic field intensity. Therefore, after the parameters are determined, a standard sample with a predetermined porosity was used to standardize the relationship between the unit volume nuclear magnetic signal and porosity. The calibrated results in the present study are shown in Fig. 3.

### 3. Results and discussion

#### 3.1. Influence of exposed time on free chloride concentration of concrete with different admixtures

The free chloride concentration in concrete in relation to the depth is shown in Figs. 4–6 for PC, SF and FA concretes, respectively, in

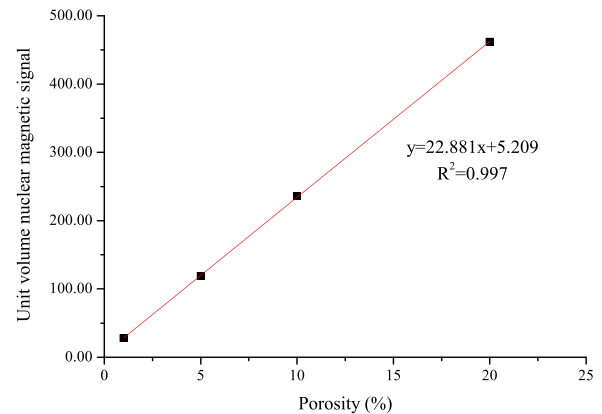


**Fig. 3.** Relationship between unit volume signal and porosity of a standard sample.

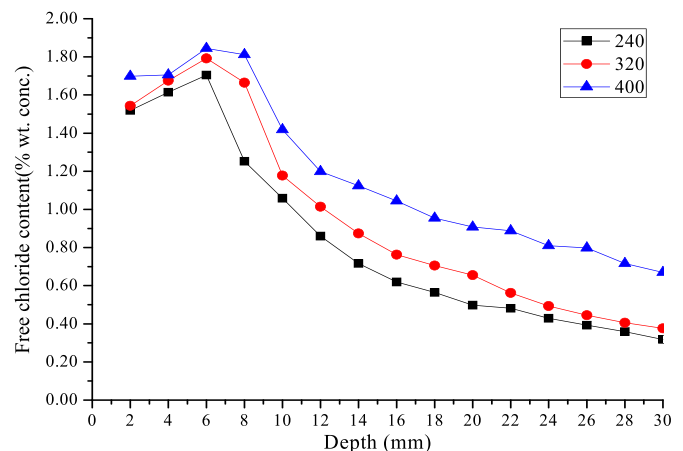


**Fig. 4.** Free chloride concentration profile of reference concrete specimen A1 at three different times.

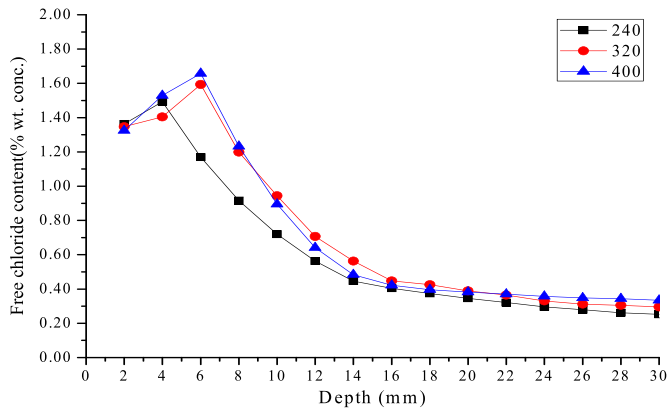


Fig. 5. Free chloride concentration profile of SF concrete specimen A3 at three different times.

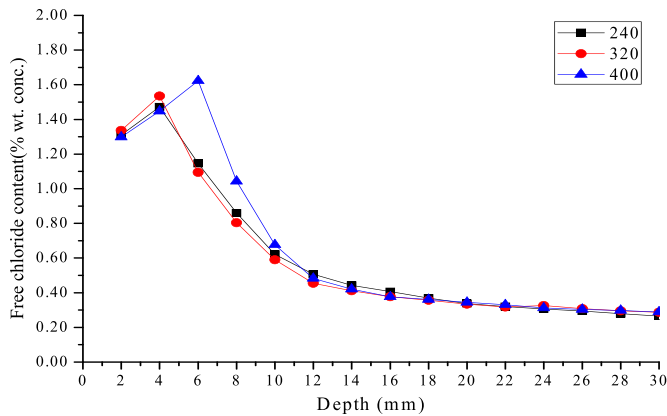


Fig. 6. Free chloride concentration profile of FA concrete specimen A4 at three different times.

which each concentration plotted represents the average value of the measured concentrations in five repeated tests.

As it can be observed from these figures, there is an increasing trend of chloride concentration at identical depths in concretes with exposed time, but the rate of the increase seems different for different mixtures. It is noted that the concrete with FA (specimen A4) or (SF specimen A3) exhibits significantly lower free chloride content than that of reference concrete A1. This indicates that both FA and SF can improve the chloride-penetration resistance of concrete (Thomas and Bamforth, 1999).

In a dry-wet cycling environment, both diffusion and capillary suction will occur in concrete. As a consequence, a “concrete skin” layer which not follow a diffusion process and an internal bulk zone that follows a diffusion process will appear. Thus, apart from the diffusion zone there is a convection zone and the highest chloride concentration is not at the surface but at an inner place, owing to wetting and drying interaction (Hong and Hooton, 2000; Yu et al., 2015; Sadati et al., 2015; Guimarães and Helene, 2008). The convection zone depths of chloride of the tested specimens can be seen in Figs. 4–6. The mean value of convection zone depth of chloride is about 4–6 mm, but will increase slowly with the exposed time. Note that the distribution profiles of chloride concentrations shown in Figs. 4–6 are for concrete specimens exposed to the simulated chloride environment. Therefore, there is an obvious consistency of the free chloride ion concentration curve in the natural and simulated environment, showing that the simulated environment can achieve the same erosion and simulation effect.

Table 4 Chloride diffusion coefficients in different concrete mixes.

Code	Chloride diffusion coefficient ( $\times 10^{-12} \text{m}^2/\text{s}$ )		
	240d	320d	400d
A1	1.449	1.024	0.848
A2	0.980	0.543	0.440
A3	1.063	0.643	0.348
A4	0.812	0.430	0.196
A5	0.678	0.374	0.235

3.2. Influence of admixtures on chloride diffusion coefficient of concrete

Fick's second law of diffusion is commonly used to fit the experimentally obtained chloride concentration profile in concrete (Liu et al., 2016) to determine the chloride diffusion coefficient. If the diffusion zone is not from the surface of concrete, but from the place  $x_c$ , where  $x_c$  is the convection zone depth, and the initial chloride concentration in concrete is zero, then the chloride concentration profile in the diffusion zone can be expressed as follows:

$$C_{x,t} = C_{sm} \left[ 1 - \text{erf} \left( \frac{x - x_c}{2\sqrt{D_a t}} \right) \right] \tag{5}$$

where  $C_{x,t}$  is the chloride concentration at depth  $x$  and time  $t$ ,  $D_a$  is the apparent diffusion coefficient in concrete,  $\text{erf}(\cdot)$  is the error function,  $C_{sm}$  is the peak value of the free chloride concentration in concrete.

According to Eq. (5), for given  $x_c$  and  $C_{sm}$ , one can determine the diffusion coefficient of chloride ions by using the best fit of Eq. (5) with the experimentally obtained chloride concentration profile. Table 4 shows the results obtained for different concrete mixes with identical w/c ratio at different exposure times.

The results given in Table 4 show that, under the artificial simulated chloride environment the chloride diffusion coefficient in all tested concretes decreases with the exposure time (Khanzadeh-Moradillo et al., 2015). Fig. 7 graphically plots the variation of the chloride diffusion coefficient with the exposure time for concretes with different admixtures.

It can be seen from Table 4 and Fig. 7 that, the addition of minerals in concrete can reduce the chloride diffusion coefficient of the mixed concrete with exposed time effectively. However, different minerals have different performances. Compared to SF, FA is more effective in reducing chloride diffusion coefficient. For example, after 240, 320, 400 days exposure duration, the concrete with the admixture FA (A4) has lower chloride diffusion coefficient of 23.6% and 33.1% and 43.7%

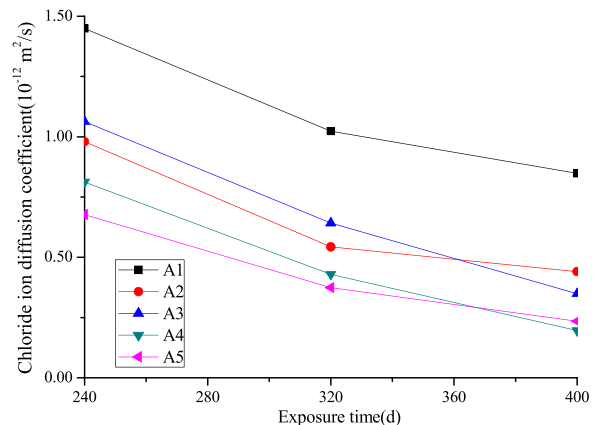


Fig. 7. Variation of chloride diffusion coefficient of tested concrete with exposed time.

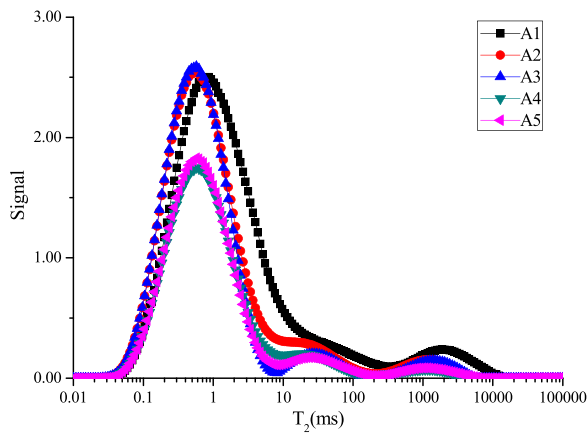


Fig. 8.  $T_2$  spectrum change of concrete specimens after exposure 240 d in simulated environment.

than that of SF concrete A3, respectively. This illustrates that, as the exposure time increases, the effect of FA becomes more significant. The reason for this is likely due to its aggravated secondary hydration.

It is noted that, after 400 d exposure duration, the chloride diffusion coefficients of concrete A2, A3, A4 and A5 are 48.1%, 59.0%, 76.9% and 72.3% lower than that of concrete A1, respectively. For all of the tested concretes from exposure 240 d to 400 d, the chloride diffusion coefficients were dropped by 41.5%, 55.1%, 67.3%, 75.9% and 65.3%, respectively. This demonstrates that the effect of FA (A4) to decrease the chloride diffusion coefficient of concrete is better in 400 d.

### 3.3. The relationship between porosity and chloride diffusion coefficient

The  $T_2$  spectrum and the unit volume nuclear magnetic signal of the tested concretes after the exposure of 240 d and 400 d are shown in Fig. 8 and Fig. 9.

It can be seen from Fig. 8 and Fig. 9 that, the signal peaks of the concretes with admixtures are all lower than that of A1, and the emergence time of the peak of the concrete with admixture is earlier than that of A1, which means that the addition of admixtures can decrease the quantity of large pores in concrete. According to the principle of NMR, the total area of each distribution curve represents the total pore water content in the tested concrete, that is, the porosity of the tested concrete. So, by comparing the area of the  $T_2$ , one can identify the effect of the added admixture on the porosity reduction of the concrete.

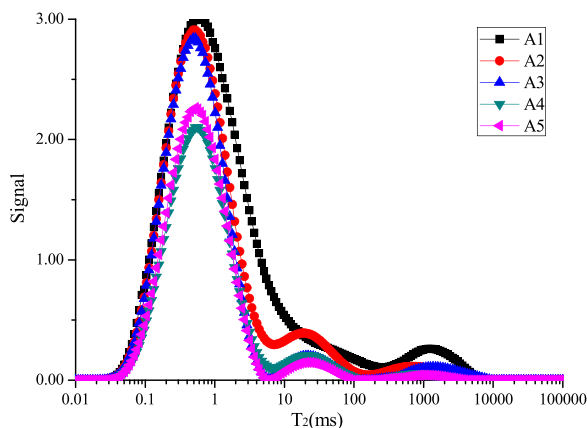


Fig. 9.  $T_2$  spectrum change of concrete specimens after exposure 400 d in simulated environment.

Table 5  
Signal and porosity of the specimens by NMR.

Specimens	Time (d)	Signal value	Porosity (%)
A1	240	221	9.41
	320	206	8.79
	400	187	7.95
A2	240	228	9.74
	320	155	6.53
	400	145	6.12
A3	240	209	8.90
	320	166	7.01
	400	123	5.15
A4	240	150	6.31
	320	102	4.25
	400	94	3.87
A5	240	144	6.27
	320	134	4.19
	400	110	4.28

According to the calibrated relationship between the unit volume nuclear magnetic signal and the porosity of the specimen, the porosities of individual tested specimens are calculated and the corresponding results are given in Table 5.

It can be observed from Table 5 that the addition of minerals in concrete can reduce the overall porosity of the mixed concrete, and thus can reduce the chloride diffusion coefficient of the mixed concrete. It seems that A4 or A5 has the lowest porosity for 240, 320 or 400 day exposure; whereas A2 or A3 has the highest porosity for the same exposure period. The time-varying trend of porosity of concretes with different admixtures with exposure time in the artificial simulation experiment is shown in Fig. 10.

The results shown in Table 5 and Fig. 10 indicated that the porosities of concrete with admixtures decreased generally with the exposure time except for the specimen A5 after exposure 320 d. The result also shows that, the longer exposure time will lead to a more reduction of porosity. Note that the sampling and/or the error of NMR test may lead to the abnormal porosity of specimen A5 after exposure 320 d, in which the sampling for NMR test is only one specimen, whereas the calculated chloride diffusion coefficient in concrete is based on the mean value of the five identical specimens.

The results described above demonstrate that there is a direct correlation between the porosity and the chloride diffusion coefficient of concrete, except for the concrete A2 after exposure 240 d. The latter could be the dense net, which can limit the emerging of the micro-crack in BF concrete, and lead to the abnormal phenomenon mentioned above (Dias and Thaumaturgo, 2005).

The data shown in Table 5 and Fig. 10 also suggest that the reduction rate of the porosity and chloride diffusion coefficient is not

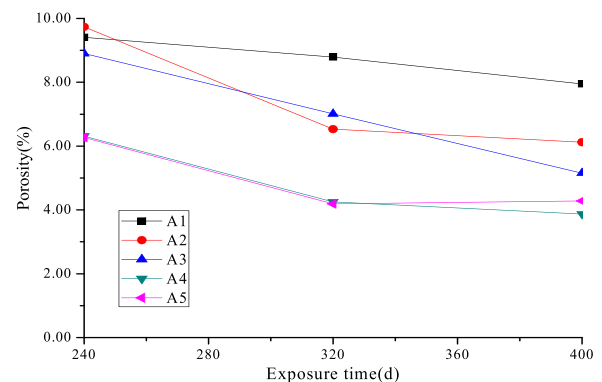


Fig. 10. Time-varying trend of the porosity of specimens with different admixtures.

**Table 6**  
Percentage of different aperture radius in total porosity of the specimens by NMR.

Specimens	Time (d)	10–100 nm (%)	Contributive porosity (%)	100–1000 nm (%)	Contributive porosity (%)
A1	240	42.27	3.98	40.05	3.77
	320	46.03	4.05	37.81	3.32
	400	50.03	3.98	33.72	2.68
A2	240	56.44	5.50	29.56	2.88
	320	59.02	3.85	26.62	1.74
	400	59.58	3.65	26.16	1.60
A3	240	62.39	5.55	25.66	2.28
	320	66.04	4.63	22.28	1.56
	400	67.17	3.46	21.93	1.13
A4	240	56.41	3.56	30.86	1.95
	320	61.63	2.62	27.87	1.18
	400	63.25	2.45	26.24	1.02
A5	240	58.86	3.69	28.58	1.79
	320	60.47	2.53	29.13	1.22
	400	67.62	2.89	24.18	1.04

simply linear to the exposure time in the dry-wet cycling chloride environment. For instance, from exposure 240 d to 320 d, the porosity of concrete A1 to A5 decreased by 6.6%, 33.0%, 21.2%, 32.6% and 33.1%, but the chloride diffusion coefficient of concrete A1 to A5 decreased by 29.4%, 44.5%, 39.5%, 47.1% and 44.8%, respectively.

Moreover, specimens FA (A4) and FA/SF (A5) will generate aluminates during the hydration process, which can combine chloride ions thus decrease the chloride concentration in concrete and reduce the chloride diffusion coefficient (Arya et al., 1990). Taking A4 for instance, from 240 to 320 days exposures the porosity had fallen 32.6% and the chloride diffusion coefficient of A4 had fallen 47.1%. From 320–400 days exposure, the porosity and chloride diffusion coefficient of specimen A4 reduces by 8.9% and 54.3%, respectively. The phenomenon also shows that the total porosity is not the only influence factor for the chloride diffusion coefficient of concrete, indicating the complex of the mixed concrete.

### 3.4. The aperture distribution and influence on permeability of concrete

Table 6 shows the experimental data for the percentage of pores of radius 10–100 nm and 100–1000 nm in terms of the total porosity measured by using the NMR for the tested concretes, in which the

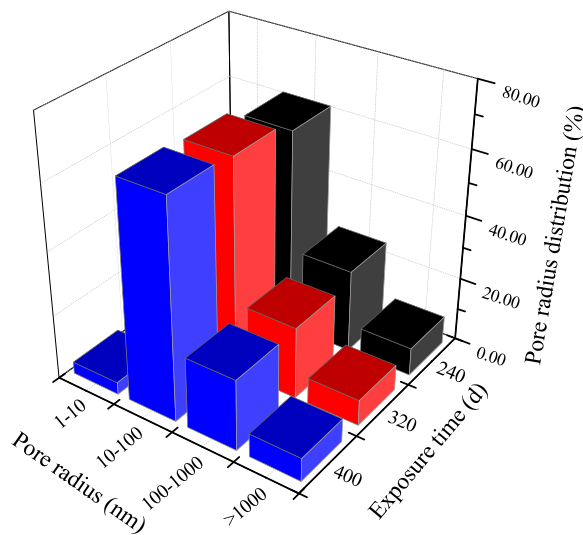


Fig. 11. Pore-size distribution for SF concrete A3 after different exposure time.

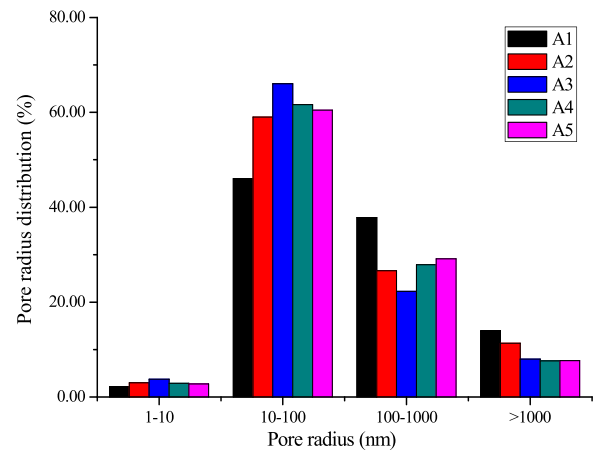


Fig. 12. Pore-size distribution for different concretes after exposure 320 d.

contributive porosity is the product of percentage of the radius in total porosity and the porosity shown in Table 5.

It is observed from Table 6 that the percentage of pores of radius 10–100 nm increases with the time but the percentage of pores of radius 100–1000 nm decreases with the time.

Fig. 11 shows the corresponding pore-size distribution for specimen SF (A3) after different exposure times. Fig. 12 presents the corresponding pore-size distribution for different concretes after exposure 320 d.

The results show that the addition of SF or FA can decrease the pores of radius 100–1000 nm in concrete and thus increase the resistance of concrete against the chloride ingress. According to the data shown in Tables 4–6, a relationship between the chloride diffusion coefficient and the total porosity, the contributive porosity of aperture radius 10–100 nm or the contributive porosity of radius 100–1000 nm in concrete can be obtained by using the linear fit. Fig. 13 shows the fitted linear relationship between the chloride diffusion coefficient and the contributive porosity of pore radius 100–1000 nm.

The linear relationship between the porosity and the chloride diffusion coefficient demonstrates that the influence of contributive porosity of pore radius 100–1000 nm on chloride diffusion coefficient is more than that of total porosity of concrete. The pore of radius 100–1000 nm is harmful to reduce the permeability of concrete. Some researchers supposed that the pore > 100 nm is definitely harmful to the properties of paste (Zhang et al., 2016; Oltulu and Sahin, 2014). There is positive correlation between the chloride diffusion coefficient and the contributive porosity of pore radius 100–1000 nm in the concrete. In other words, the high contributive porosity in the concrete will certainly lead to a high chloride diffusion coefficient of the concrete. Moreover, there is a negative correlation

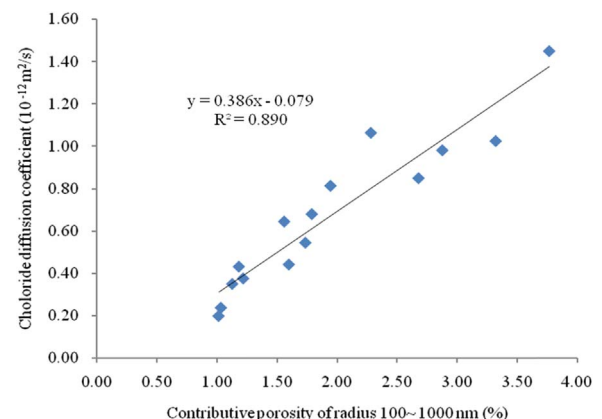


Fig. 13. Relationship between contributive porosity of pore radius 100–1000 nm and chloride diffusion coefficient in concrete.

between the chloride diffusion coefficient and the contributive porosity of radius 10–100 nm, which is conducive to increase the anti-permeability of concrete.

#### 4. Conclusion

This paper has presented an investigation on the relation between the chloride diffusion coefficient, porosity, and pore-size distribution in concrete and the effect of exposure time on these parameters when the concrete is exposed to an artificial simulated dry-wet cycling chloride environment. Based on the experimentally obtained results and the analysis of experimental data, the following conclusions can be drawn.

- (1) Concrete porosity and chloride diffusion coefficients exhibit a decrease trend with the exposure time when the concrete is exposed to the artificial simulated dry-wet cycling environment. The tested concretes with different admixtures can reduce the chloride diffusion coefficient and the overall porosity significantly, in which the decreased effect of SF in concrete on porosity is the most obvious, and the decreased effect of FA on chloride diffusion coefficient of concrete is the most significant, especially at the later stage.
- (2) There is a better correlation between the chloride diffusion coefficient and total porosity in concrete. However, the total porosity is not the only influence factor on the chloride diffusion coefficient; the pore-size distribution also has a great influence on the permeability of concrete.
- (3) The influence of the contributive porosity of pore radius 100–1000 nm in concrete on chloride diffusion coefficient is more than that of total porosity of concrete. The increase of contributive porosity in concrete will result in a larger chloride diffusion coefficient. There is a correlation between the contributive porosity of radius 100–1000 nm in concrete and the chloride diffusion coefficient.
- (4) The chloride diffusion coefficient is found to decrease with the exposure time for concretes with minerals. Thus, the addition of minerals in concrete can increase the durability of the mixed concrete to against the chloride penetration.

#### Acknowledgements

This work was financially supported by the National Natural Science Foundation of Zhejiang Province (Nos. LY17E090007 and LY13E090008) and the National Natural Science Foundation of China (Nos. 50879079 and 51279181). The supports are gratefully acknowledged.

#### References

Arya, C., Buenfeld, N.R., Newman, J.B., 1990. Factors influencing chloride binding in concrete. *Cem. Concr. Res.* 20 (2), 291–300.

Audenaert, K., Yuan, Q., Schutter, G. De, 2010. On the time dependency of the chloride migration coefficient in concrete. *Constr. Build. Mater.* 24, 396–402.

Bayer, J.V., Jaeger, F., Schaumann, G.E., 2010. Proton nuclear magnetic resonance (NMR) relaxometry in soil science applications. *Open Magn. Reson. J.* 3, 15–26.

Boddy, A., Bentz, E., Thomas, M.D.A., et al., 1999. An overview and sensitivity study of a multimechanistic chloride transport model. *Cement Concr. Res.* 29 (6), 827–837.

Camacho, J.B., Abdelkader, S.M., Pozo, E.R., et al., 2014. The influence of ion chloride on concretes made with sulfate-resistant cements and mineral admixtures. *Constr. Build. Mater.* 70, 483–493.

Coates, G.R., Xiao, L.Z., Prammer, M.G., 1999. *NMR Logging Principles and Application*. Halliburton Energy Services Publication, Houston.

Cook, R.A., Hover, K.C., 1999. Mercury porosimetry of hardened cementpastes. *Cem. Concr. Res.* 29 (6), 933–943.

Costa, A., Appleton, J., 1999. Chloride penetration into concrete in marine environment—Part II: prediction of long term chloride penetration. *Mater. Struct.* 32, 354–359.

Diamond, S., 2000. Mercury porosimetry: an inappropriate method for the measurement of pore size distributions in cement-based materials. *Cem. Concr. Res.* 30 (10), 1517–1525.

Dias, D.P., Thaumaturgo, C., 2005. Fracture toughness of geopolymeric concretes reinforced with basalt fibers. *Cem. Concr. Compos.* 1, 49–54.

Dong, S.G., Zhang, G.J., Hou, L.Y., et al., 2015. Analysis of the relationship between the porosity and the salt freezing resistance of concrete by NMR data. *J. Chin. Electron Microsc. Soc.* 05, 428–432.

Gao, J.M., Yu, Z.X., Song, L.G., et al., 2013. Durability of concrete exposed to sulfate attack under flexural loading and drying–wetting cycles. *Constr. Build. Mater.* 39, 33–38.

Guimarães, A.T.C., Helene, P.R.L., 2008. Confirmation of a model to predict chloride ion penetration with peak over time. In: *Proceedings of the Fifth ACI/CANMET International Conference on High-Performance Concrete Structures and Materials*. Manaus, AM, Brazil, 253, pp. 155–164.

Hong, K., Hooton, R.D., 2000. Effects of fresh water exposure on chloride contaminated concrete. *Cement Concr. Res.* 30, 1199–1207.

Jaeger, F., Bowe, S., Vanas, H., et al., 2009. Evaluation of  $^1\text{H}$  NMR relaxometry for the assessment of pore-size distribution in soil samples. *Eur. J. Soil Sci.* 60, 1052–1064.

Ji, Y.L., Sun, Z.P., Yang, X., et al., 2015. Assessment and mechanism study of bleeding process in cement paste by  $^1\text{H}$  low-field NMR. *Constr. Build. Mater.* 100, 255–261.

Jia, L.F., Shi, C.J., Pan, X.Y., et al., 2016. Effects of inorganic surface treatment on water permeability of cement-based materials. *Cem. Concr. Compos.* 67, 85–92.

Khanzadeh-Moradillo, M., Meshkini, M.H., Eslamdoost, E., et al., 2015. Effect of wet curing duration on long-term performance of concrete in tidal zone of marine environment. *Int. J. Concr. Struct. Mater.* 9 (4), 487–498.

Liu, P., Yu, Z.W., Lu, Z.H., et al., 2016. Predictive convection zone depth of chloride in concrete under chloride environment. *Cem. Concr. Compos.* 72, 257–267.

Loukili, A., Khelidj, A., Richard, P., 1999. Hydration kinetics, change of relative humidity, and autogenous shrinkage of ultra-high-strength concrete. *Cem. Concr. Res.* 29 (4), 577–584.

Mangat, P.S., Molloy, B.T., 1994. Prediction of long term chloride concentration in concrete. *Mater. Struct.* 27, 338–346.

Mohammed, M.K., Dawson, A.R., Thom, N.H., 2014. Macro/micro-pore structure characteristics and the penetration of self-compacting incorporating different types of filler and mineral admixture. *Constr. Build. Mater.* 72, 83–93.

Oltulu, M., Sahin, R., 2014. Pore structure analysis of hardened cement mortars containing silica fume and different nano-powders. *Constr. Build. Mater.* 53, 658–664.

Papakonstantinou, K.G., Shinozuka, M., 2013. Probabilistic model for steel corrosion in reinforced concrete structures of large dimensions considering crack effects. *Eng. Struct.* 57, 306–326.

Pipilikaki, P., Beazi-Katsion, M., 2009. The assessment of porosity and pore size distribution of limestone Portland cement pastes. *Constr. Build. Mater.* 23, 1966–1970.

Sadati, S., Arezoumandi, M., Shekarchi, M., 2015. Long-term performance of concrete surface coatings in soil exposure of marine environments. *Constr. Build. Mater.* 94, 656–663.

Simčič, T., Pejovnik, S., Schutter, G. De, et al., 2015. Chloride ion penetration into fly ash modified concrete during wetting–drying Cycles. *Constr. Build. Mater.* 93, 1216–1223.

Song, L.G., Sun, W., Gao, J.M., 2013. Time dependent chloride diffusion coefficient in concrete. *J. Wuhan. Univ. Technol.-Mater.* 28 (2), 314–319.

Tang, L., Nilsson, L.O., 1995. A discussion of the paper “calculation of chloride diffusivity in concrete from migration experiments, in non-steady-state conditions” by C. Andrade, D. Cervigón, A. Recuero and O. Río. *Cem. Concr. Res.* 25, 1133–1137.

Thomas, M.D.A., Bamforth, P.B., 1999. Modeling chloride diffusion in concrete: effect of fly ash and slag. *Cem. Concr. Res.* 29 (4), 487–495.

Tian, H.H., Wei, C.F., Wei, H.Z., et al., 2014. Freezing and thawing characteristics of frozen soils: bound water content and hysteresis phenomenon. *Cold Reg. Sci. Technol.* 103, 74–81.

Valipour, M., Shekarchi, M., Ghods, P., 2014. Comparative studies of experimental and numerical techniques in measurement of corrosion rate and time-to-corrosion-initiation of rebar in concrete in marine environments. *Cem. Concr. Compos.* 48, 98–107.

Wang, X.X., Shen, X.D., Wang, H.L., et al., 2015. Nuclear magnetic resonance analysis of concrete-lined channel freeze-thaw damage. *J. Ceram. Soc. Jpn.* 123 (1), 43–51.

Xiao, L.Z., 1998. *NMR Imaging Logging Principles and Applications*. Science Press, Beijing.

Yu, L.W., François, R., Dang, V.H., et al., 2015. Structural performance of RC beams damaged by natural corrosion under sustained loading in a chloride environment. *Eng. Struct.* 96, 30–40.

Yu, Z.W., Chen, Y., Liu, P., et al., 2015. Accelerated simulation of chloride ingress into concrete under drying–wetting alternation condition chloride environment. *Constr. Build. Mater.* 93, 205–213.

Zhang, B., 1998. Relationship between pore structure and mechanical properties of ordinary concrete under bending fatigue. *Cem. Concr. Res.* 28 (5), 699–712.

Zhang, J.Z., Wang, J.Z., Kong, D.Y., 2010. Chloride diffusivity analysis of existing concrete based on Fick’ second law. *J. Wuhan. Univ. Technol.* 25 (1), 142–146.

Zhang, M.Z., Ye, G., 2010. Modelling of time dependency of chloride diffusion coefficient in cement paste. *J. Wuhan. Univ. Technol.* 25 (3), 687–691.

Zhang, Z.Q., Zhang, B., Yan, P.Y., 2016. Hydration and microstructures of concrete containing raw or densified silica fume at different curing temperatures. *Constr. Build. Mater.* 121, 483–490.